QUANTUM GASES

Universal scaling of the dynamic BKT transition in quenched 2D Bose gases

Shinichi Sunami[1]*, Vijay Pal Singh[2,3], David Garrick[1], Abel Beregi[1], Adam J. Barker[1], Kathrin Luksch[1], Elliot Bentine[1], Ludwig Mathey[4,5], Christopher J. Foot[1]

The understanding of nonequilibrium dynamics in many-body quantum systems is a fundamental issue in statistical physics. Experiments that probe universal properties of these systems can address such foundational questions. In this study, we report the measurement of universal dynamics triggered by a quench from the superfluid to normal phase across the Berezinskii-Kosterlitz-Thouless transition in a two-dimensional (2D) Bose gas. We reduced the density by splitting the 2D gas in two, realizing a quench across the critical point. The subsequent relaxation dynamics were probed with matter-wave interferometry to measure the local phase fluctuations. We show that the time evolution of both the phase correlation function and vortex density obeys universal scaling laws. This conclusion is supported by classical-field simulations and interpreted by means of real-time renormalization group theory.

The relaxation dynamics of a many-body system that is quenched out of equilibrium display a wide range of scenarios, from simple exponential decay to relaxation through metastable or prethermalized states (*1*, *2*), including phenomena such as pattern formation (*3*), and the absence of thermalization (*4*). Systems that are quenched across a phase transition are particularly intriguing because of their universal self-similar behavior, expected in systems as diverse as superfluid helium (*5*), liquid crystals (*6*), biological cell membranes (*7*), the early universe (*8*), and cold atoms (*9*, *10*). There are numerous theoretical challenges in the treatments of nonequilibrium dynamics [e.g., (*11*)], and this motivates in-depth experimental studies to guide and test theories.

For this purpose, ultracold gases have emerged as a platform of unprecedented control and tunability, serving as quantum simulators for the investigation of many-body dynamics. This approach has led to the observation of Kibble-Zurek (KZ) scaling (*12*–*15*) and universal scaling laws (*16*–*18*) after a quench. Despite theoretical interest (*19*–*21*), universal critical dynamics in nonequilibrium continuous two-dimensional (2D) quantum gases remain elusive because of the lack of precise experimental probes. We show how fluctuations of the many-body 2D system can be probed directly through the extension of local matter-wave interferometry (*22*) similar to that previously used to probe the local phase fluctuations of near-integrable 1D

[1]Clarendon Laboratory, University of Oxford, Oxford OX1 3PU, UK. [2]Institut für Theoretische Physik, Leibniz Universität Hannover, 30167 Hannover, Germany [3]Quantum Research Centre, Technology Innovation Institute, Abu Dhabi, United Arab Emirates. [4]Zentrum für Optische Quantentechnologien and Institut für Laserphysik, Universität Hamburg, 22761 Hamburg, Germany. [5]The Hamburg Centre for Ultrafast Imaging, Hamburg 22761, Germany.
*Corresponding author. Email: shinichi.sunami@physics.ox.ac.uk

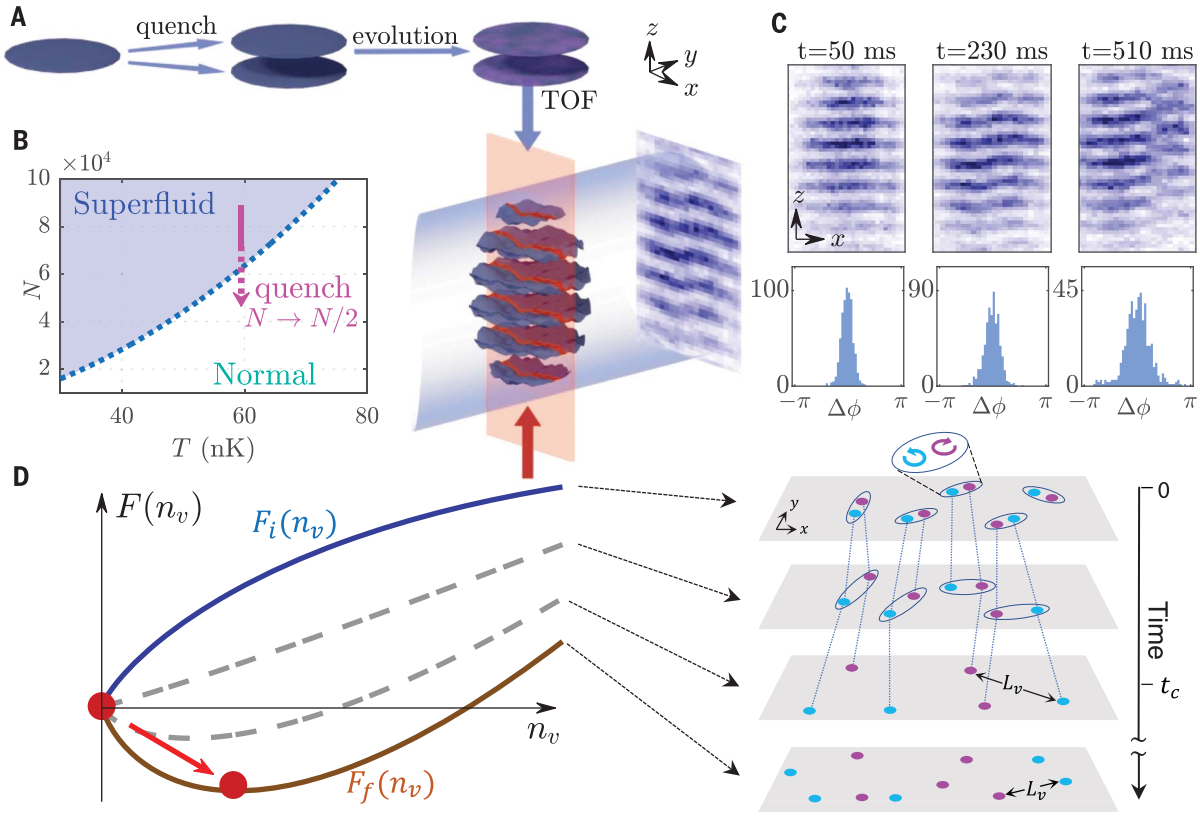

Fig. 1. Observation of nonequilibrium dynamics in 2D Bose gases with matter-wave interferometry. (**A**) A 2D superfluid is split into two daughter clouds, thereby quenching through the BKT transition. The two clouds evolve for time *t* and are released to produce matter-wave interference after a TOF. Local phase fluctuations are observed by optically pumping the slice (red sheet) and then performing absorption imaging. (**B**) Equilibrium phase diagram of trapped 2D Bose gases (*27*). The quench forces the system out of equilibrium toward the normal phase. (**C**) (Top) Examples of interference images. Phase dislocation caused by a vortex is visible in the image at 510 ms. (Bottom) The histograms show the phase differences, $\Delta\phi = \phi(x) - \phi(x')$, at $|x - x'| = 5$ μm, from 45 experimental runs. The decreasing height and increasing width indicate increased phase fluctuations. (**D**) (Left) Free energies $F_i(n_v)$ and $F_f(n_v)$ (continuous lines) in equilibrium for the initial and final conditions of the quench, with their minima indicated by red points (*38*). After the quench, the system undergoes nonequilibrium dynamics (dashed lines) and relaxes toward the state with nonzero free-vortex density, n_v. (Right) Illustration of the dynamics, showing the transition between a scale-invariant phase supported by bound vortex-antivortex pairs and the broken scale-invariant phase characterized by free vortices with the mean vortex-vortex distance L_v, where t_c is the crossover time.

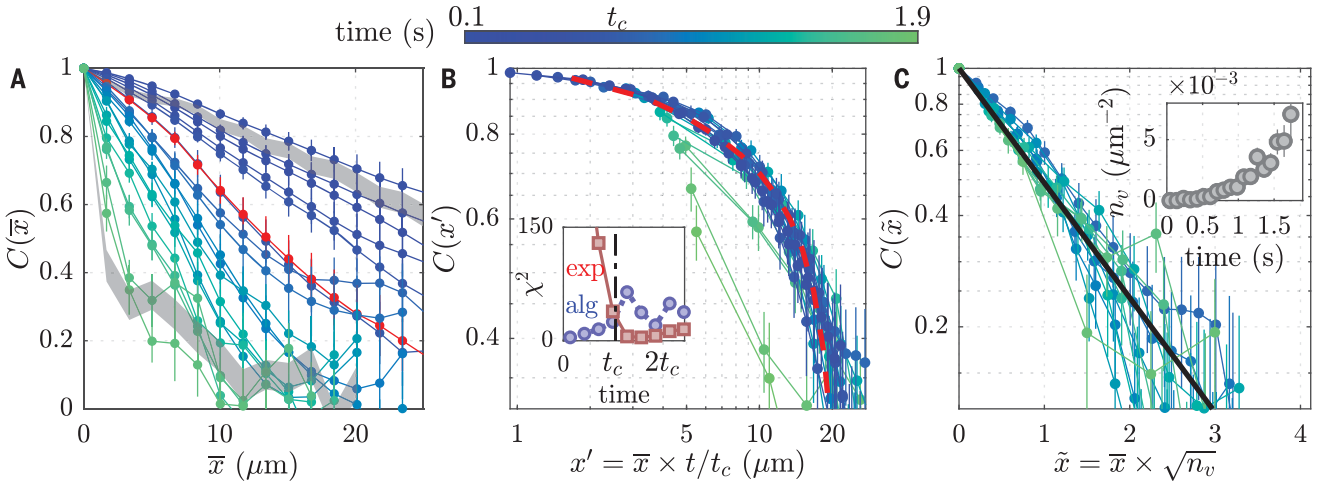

Fig. 2. Nonequilibrium scaling dynamics of the correlation function. (**A**) Relaxation dynamics of the phase correlation function $C(\bar{x})$ measured after the quench for the initial reduced temperature, $\tilde{T} = 0.34$, where $C(\bar{x})$ is an average over 45 realizations or more, and the error bars denote standard error. The data immediately after the critical time, t_c, are indicated by the red curve. For comparison, the measured data for equilibrium 2D gases (*22*) are shown by the gray curves: $\tilde{T} = 0.41$ (top) in the superfluid regime and $\tilde{T} = 0.61$ (bottom) in the normal regime. (**B**) Linear scaling of length $x' = \bar{x}t/t_c$, according to time t/t_c, results in a collapse toward a common curve for time evolution up to $t \sim 1$ s. This universal function is compatible with the expected behavior at the crossover in equilibrium (red dashed line), including the effect of inhomogeneity (*27*). At long times, deviations are observed (green points), indicating the breaking of scale invariance. (Inset) The χ^2 values for the algebraic and exponential fit functions (*27*). (**C**) Rescaling of the distance $\tilde{x} = \bar{x}\sqrt{n_v(t)}$, according to the vortex density $n_v(t)$, results in a collapse of the curves for times $t > 1$ s. Scaling behavior is compatible with an exponential decay (black solid line). (Inset) $n_v(t)$.

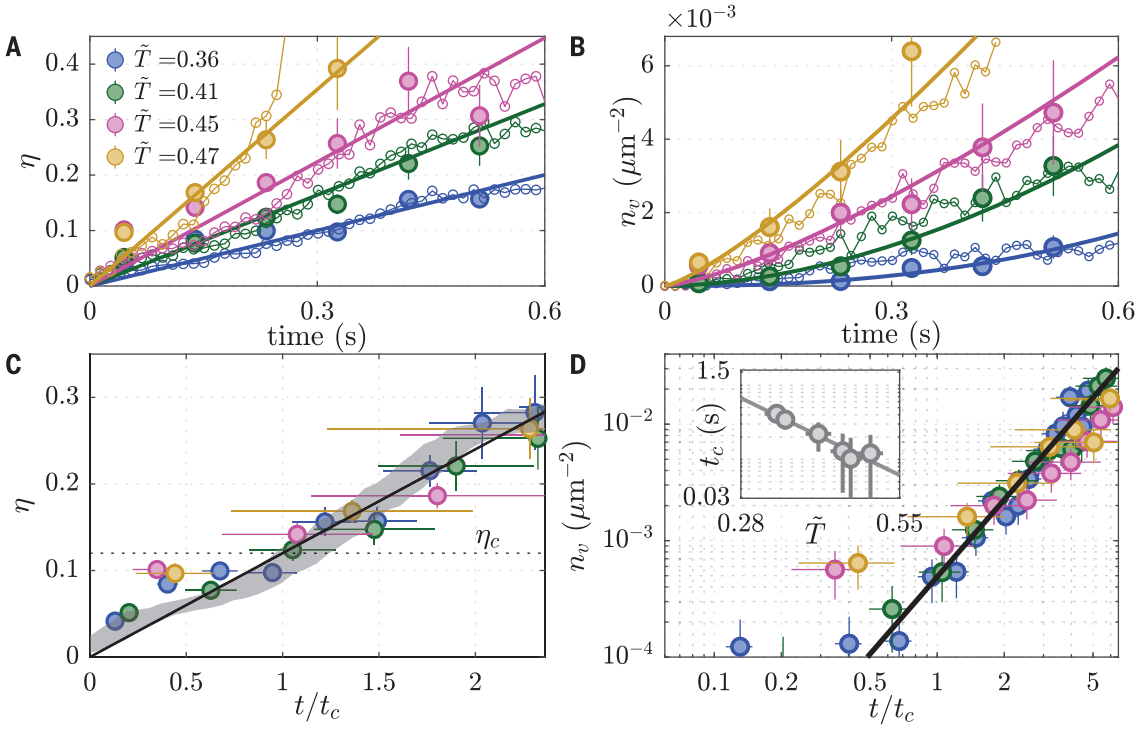

Fig. 3. Universal behavior across the dynamic BKT transition. (**A**) Measured algebraic exponent $\eta(t)$ after the quench at different initial $\tilde{T}$ (filled circles), where the equilibrium critical temperature, $\tilde{T}_c = 0.53$, is crossed by the quench (*22*). Open circles indicate the corresponding simulation results (*27*). Solid lines indicate linear fits to the experimental data, and error bars denote standard fit errors. (**B**) Time evolution of the measured (filled circles) and simulated (open circles) vortex density, $n_v(t)$. The solid lines are power-law fits to the experimental data. Error bars are statistical, given by the square root of observed vortex number. (**C**) Time evolution $\eta(t/t_c)$, scaled according to the $\tilde{T}$-dependent crossover time, t_c. The horizontal error bars arise from the uncertainty in t_c. This universal behavior is used to determine the critical exponent, $\eta_c = 0.13(1)$ (horizontal dotted line), at $t/t_c = 1$. The gray shaded curve indicates the simulation result at $\tilde{T} \sim 0.4$, and the solid line is a guide for the eye. (**D**) Scaled time evolution $n_v(t/t_c)$, plotted on a log-log scale, displays a universal growth after t_c. Black solid line is the fit with power law $n_v \propto t^{2\nu}$, which yields $\nu = 1.1(1)$. (Inset) Dependence of t_c on $\tilde{T}$, with a solid line as a guide for the eye.

systems (*1*, *2*). A feature of 2D systems is that, unlike 1D systems, they exhibit phase transitions with associated critical phenomena. An especially interesting case is that of the critical dynamics across the Berezinskii-Kosterlitz-Thouless (BKT) transition (*23*–*25*), when the system is quenched from the superfluid to the normal phase, the opposite of commonly used quenches that move from the disordered to ordered phase. Real-time renormalization-group (RG) theory and truncated Wigner simulations (*19*) predict that the relaxation occurs

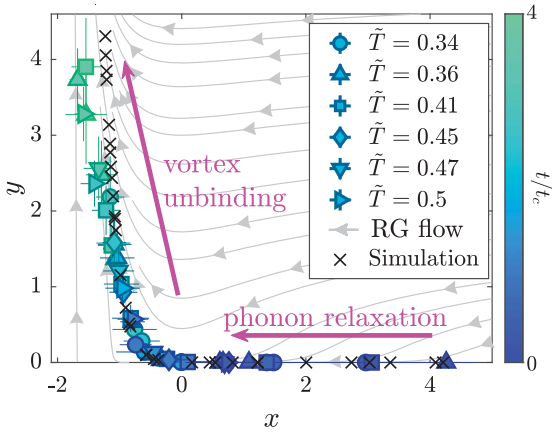

Fig. 4. Real-time renormalization group flow and measurements. Gray lines with arrows are the RG flow of the parameters $x = 1/(2\eta) - 1/(2\eta_c)$ and $y = \sqrt{2}\pi g$ [Eqs. 1 and 2 and (*27*)]. These results are compared with the experimental data for six different initial temperatures, with the time scaled by the corresponding $\tilde{T}$-dependent crossover time, t_c. Error bars denote standard errors propagated from the values for η and n_v. The results from a numerical simulation at $\tilde{T} = 0.47$ are shown as black crosses, where the deviation from experimental data at small x is attributed to the slow trap-induced heating (*27*).

through a reverse-Kibble-Zurek–type mechanism in which delayed vortex proliferation results in a metastable supercritical phase. For equilibrium systems, the BKT transition is driven by the unbinding of vortex-antivortex pairs (*22*, *26*), underscoring the topological nature of the transition. This transition is characterized by a change of the functional form of the correlation function from a power law deep in the superfluid regime, $g_1(\mathbf{r}, \mathbf{r'}) = \langle \Psi(\mathbf{r})^\dagger \Psi(\mathbf{r'}) \rangle \propto |\mathbf{r} - \mathbf{r'}|^{-\eta}$, to exponential deep in the normal regime, $g_1(\mathbf{r}, \mathbf{r'}) \propto e^{-|\mathbf{r}-\mathbf{r'}|/r_0}$, where $\Psi(\mathbf{r})$ is the bosonic field operator at position vector $\mathbf{r}$, η is the algebraic exponent, and r_0 is a correlation length. A similar change of the functional form of the single-particle correlation function is also expected for the dynamical BKT transition. However, this change is expected to occur as a smooth crossover between the two phases (*19*, *27*).

Here, we studied the critical dynamics across the BKT transition by quenching a 2D Bose gas from the superfluid to the normal phase by splitting it in two. Using spatially resolved matter-wave interferometry, we measured the first-order correlation function and vortex density to analyze their relaxation dynamics. We found that relaxation occurs through a two-step process involving phonon relaxation followed by dynamical vortex proliferation. We demonstrated universal scaling laws for the algebraic exponent and vortex density by performing measurements at different initial conditions. Both real-time RG theory (*19*, *28*) and classical-field simulations are in good agreement with our measurements.

Matter-wave interferometry after a quench

Our experiments began with a single, pancake-shaped quasi-2D Bose gas in the superfluid regime, consisting of $N \approx 9 \times 10^4$ atoms of ^{87}Rb at reduced temperatures in the range $\tilde{T} = 0.34 - 0.5$; here, $\tilde{T} \equiv T/T_0$ is the ratio of the initial temperature, T, and the critical temperature $T_0 = \sqrt{6N}(\hbar\omega_r/\pi k_B) \approx 120$ nK of a non-interacting trapped gas (*29*), where $\omega_r/2\pi = 11$ Hz is the radial trapping frequency, $\hbar$ is the reduced Planck constant, and k_B is the Boltzmann constant. The quench is implemented by a rapid splitting of the system in a multiple-RF–dressed potential (*27*, *30*–*32*) (Fig. 1A), which results in a pair of decoupled clouds, each with atom number $N' = N/2$, trapped in the two minima of a double-well potential. Each well has a vertical-trap frequency of $\omega_z/2\pi = 1$ kHz, hence the dimensionless 2D interaction strength is $\tilde{g} = \sqrt{8\pi}a_s/\ell_0 = 0.076$ (*27*), where a_s is the 3D s-wave scattering length and $\ell_0 = \sqrt{\hbar/(m\omega_z)}$ is the harmonic oscillator length along z for an atom of mass m. The initial reduced temperature, $\tilde{T}$, is chosen to be close to the equilibrium critical point at $\tilde{T}_{c,eq} = 0.53$ so that the value after splitting, $\tilde{T}'/\tilde{T} = 1.67$, corresponds to the normal phase (*27*). To investigate the dynamics, we let each cloud evolve independently for time t before performing a time-of-flight (TOF) expansion of $t_{TOF} = 16$ ms, after which we detected the matter-wave interference that encodes the in situ relative phase fluctuation, $\phi(x)$, of two clouds along a line that goes through the center of the cloud. Interference images and histograms of spatial phase fluctuations $\Delta\phi$ show stronger fluctuations at long evolution times (Fig. 1C). The dynamics across the BKT transition are expected to be scale invariant until the bound vortex-antivortex pairs dissociate to disrupt the phase coherence (Fig. 1D).

Relaxation dynamics

To analyze the relaxation dynamics, we used the interference pattern to determine both the correlation function and the vortex density (*22*). The phase correlation of the system between two points at locations $x - \bar{x}/2$ and $x + \bar{x}/2$, with spatial separation $\bar{x}$, is determined by $C(x - \bar{x}/2, x + \bar{x}/2) = \mathrm{Re}\left[\frac{1}{N_r}\sum_{j=1}^{N_r} e^{i\left[\phi_j(x-\bar{x}/2) - \phi_j(x+\bar{x}/2)\right]}\right]$, where the index, j, runs over $N_r = 45$ experimental repeats; $C(x - \bar{x}/2, x + \bar{x}/2) = 1$ indicates perfect correlation of phases, whereas $C(x - \bar{x}/2, x + \bar{x}/2) = 0$ denotes uncorrelated phases. For quantitative analysis, we average $C(x - \bar{x}/2, x + \bar{x}/2)$ over x within the region of clear interference fringes to obtain $C(\bar{x})$ (*33*). In (*22*), $C(\bar{x})$ of 2D Bose gases at equilibrium was found to decay exponentially in the normal regime, whereas in the superfluid regime it was found to decay algebraically with spatially varying exponent for inhomogeneous 2D gases in the superfluid regime, which is in agreement with the prediction based on local correlation approximation in (*34*).

In Fig. 2A, we show the time evolution of $C(\bar{x})$ after the quench at $t = 0$. Initially, there is almost no spatial correlation decay because the two clouds have nearly identical phases; their phases decouple within ~100 ms (*27*). After this, we observe a temporal decay of $C(\bar{x})$ for all $\bar{x}$. At longer times, we observe rapid spatial decay of correlation, indicating vanishing coherence at large distances. To determine the nature of this dynamic transition, we fit $C(\bar{x})$ with the algebraic and exponential functions that are used to characterize the equilibrium BKT transition (*22*). As the system relaxes from the initial superfluid state to the normal state, it is expected that $C(\bar{x})$ will evolve smoothly from algebraic to exponential scaling in the short- and long-time limits, respectively. At intermediate times, both power-law and exponential fitting can be used to extract physical properties of the nonequilibrium state; within the real-time RG picture, nonequilibrium systems in the crossover region are away from the fixed point and there is no direct correspondence to equilibrium systems (*19*, *35*). Indeed, at short and intermediate times, the spatial decay of the correlation function is compatible with algebraic scaling, including the effect of inhomogeneity of the system, and with exponential scaling for long times (*27*). We identified the crossover time, t_c, as the time at which the correlation function becomes better described by exponential scaling rather than algebraic (Fig. 2B, inset). Even after t_c, the χ^2 values for the power-law model remain small, supporting the description of the system with the power-law exponent η beyond t_c (*27*).

The dynamic BKT transition is expected to have self-similar dynamics with a length scale that depends linearly on time (*19*, *36*, *37*). Motivated by this, we have plotted the correlation functions with rescaled length $x' = \bar{x}t/t_c$, using $t_c \sim 0.5$ s (Fig. 2B). This shows convincingly that, except for long times, the fluctuations in the system depend only on the rescaled parameter x' through a universal function, which we found to be close to the expected function at the equilibrium BKT crossover (Fig. 2B). We found the same behavior independent of the initial condition (temperature) of the system, demonstrating the robustness of the scale-invariant behavior near the critical point (fig. S4).

At long times, scale invariance is broken by vortex excitations, which results in an emergent

length scale, $r_0 \approx 1/\sqrt{n_v}$, where n_v is the vortex density (*27*). To demonstrate this, we plotted the correlation function at long times against the rescaled distance $\tilde{x} = \bar{x}\sqrt{n_v}$ (Fig. 2C) (*37*). We obtained n_v from the occurrence of sudden jumps of phases, which indicate the presence of a vortex core (*22*, *26*, *27*). These transformed correlation functions are nearly time independent, showing that the system can be characterized by the vortex density deep in the normal regime.

Varying the initial conditions

Having verified the behavior of the dynamic BKT transition, we next analyzed its universal characteristics by varying $\tilde{T}$. The time evolution of the algebraic exponent, η, determined by using an algebraic fit to $C(\bar{x})$, exhibits a linear increase in which the increase is faster for higher $\tilde{T}$ (Fig. 3A). This shows that the dynamics are accelerated at higher $\tilde{T}$ and that the system quickly crosses over to the normal phase. This is also reflected in the measurements of the vortex density, n_v, showing a faster growth at higher $\tilde{T}$ (Fig. 3B). We found that the vortex growth follows a power-law scaling as expected from the RG predictions (fig. S8). We compared the measurements of η and n_v with the corresponding results of classical-field simulations, which give consistent dynamics (Fig. 3, A and B).

To confirm universal scaling, η and n_v have been plotted as a function of scaled time, t/t_c (Fig. 3, C and D). The time evolutions for various initial values of $\tilde{T}$ collapse onto a single curve, showing the robustness of dynamical scaling. We found a linear increase of η across $t = t_c$. In equilibrium theory, η scales approximately linearly with temperature in the superfluid regime (i.e., $\eta \propto T/4T_{\mathrm{BKT}}$) (*25*), thus connecting the temperature scale with phase fluctuations. From this linear estimate, we obtained the critical exponent $\eta_c = 0.13(1)$ at $t/t_c = 1$, close to the value $\eta_c = 0.17(3)$ found for a finite-size equilibrium system with similar experimental parameters (*22*) and different from the value of $\eta_{\mathrm{BKT}} = 0.25$ for the equilibrium BKT transition in the thermodynamic limit. The linear increase of η after $t/t_c = 1$ is a precursor of nonequilibrium superheated superfluid (*28*) as a consequence of a delayed vortex proliferation. The vortex growth after $t/t_c = 1$ exhibited universal power-law scaling $n_v \propto t^{2\nu}$, with $\nu \sim 1$; this agrees with the RG prediction, as shown in the next section.

Comparison to renormalization-group theory

We next compared the experimental results with predictions based on the real-time RG equations (*19*, *28*). These equations describe the time evolution of parameters characterizing the system from arbitrary nonequilibrium states flowing toward fixed points, which represent possible equilibrium states. For the dynamic BKT transition, the real-time RG equations are (*19*, *27*, *28*)

$$\frac{dg}{dt} = \left(2 - \frac{1}{2\eta}\right)\frac{g}{t} \tag{1}$$

$$\frac{d\eta}{dt} = \frac{\pi g^2}{16\eta t} + \gamma \tag{2}$$

where the vortex fugacity, g, is related to the vortex density by $n_v(t) = n\tilde{g}\exp[(2\ln(g/2))/(2 - 1/(2n))]$. n is the mean density within the region of interest used for fringe analysis, and $\tilde{g}$ is the interaction strength as defined previously; these parameters also determine the healing length, $\xi = 1/\sqrt{n\tilde{g}}$, characterizing the length scale of the vortex cores (*27*, *38*). This RG flow derives from the dynamical sine-Gordon model, serving as a dual model for describing the BKT transition; we have added a phenomenological heating term, γ, to account for the slow, trap-induced heating of the system (*27*). For $\eta < 1/4$, the fugacity is strongly suppressed, resulting in a linear dispersion, $\omega_k = ck$. As η increases in time, the vortex fugacity becomes relevant and increases, resulting in a dispersion, $\omega_k = c\sqrt{k^2 + 1/r_0^2(t)}$. As we have argued and demonstrated in the previous sections, this is indeed supported by the two-step scaling behavior. Furthermore, at long times, we have $1/(2\eta) \ll 2$, therefore $n_v \propto g \propto t^2$ (Fig. 3D).

In Fig. 4, the experimental observations are plotted together with the RG flow diagram of Eqs. 1 and 2. For this representation, we defined $x = 1/(2\eta) - 1/(2\eta_c)$ and $y = \sqrt{2\pi}g$. This ensures that $x_c = 0$ at $\eta = \eta_c$ independent of system sizes, where $\eta_c = 0.13(1)$ for our finite-sized system, and $\eta_c = \eta_{\mathrm{BKT}} = 1/4$ is the theoretical prediction in the thermodynamic limit. Our results follow a universal trajectory in the flow diagram. The quenched system begins at large x, where vortex excitations are suppressed and fugacity is small. Later on, nonequilibrium phonon creation drives the system toward smaller x, however still with suppressed y. As the system approaches the critical point $x_c = 0$, the onset of vortex excitation drives the transition.

Discussion and outlook

Our work provides a comprehensive understanding of nonequilibrium dynamics across the BKT transition. The experimental measurements support the real-time RG picture of universality out of equilibrium, indicating that it is an excellent starting point for the theoretical study of a wide range of many-body dynamics within the framework of RG. The results also show that our matter-wave interference technique is ideally suited for further in-depth investigation of universal dynamics in 2D systems, such as the Kibble-Zurek scaling (*8*) and nonthermal fixed points (*39*).

REFERENCES AND NOTES

1. T. Langen *et al.*, *Science* **348**, 207–211 (2015).
2. T. Schweigler *et al.*, *Nature* **545**, 323–326 (2017).
3. H. P. Zahn *et al.*, *Phys. Rev. X* **12**, 021014 (2022).
4. T. Kinoshita, T. Wenger, D. S. Weiss, *Nature* **440**, 900–903 (2006).
5. W. H. Zurek, *Nature* **317**, 505–508 (1985).
6. I. Chuang, R. Durrer, N. Turok, B. Yurke, *Science* **251**, 1336–1342 (1991).
7. S. L. Veatch, O. Soubias, S. L. Keller, K. Gawrisch, *Proc. Natl. Acad. Sci. U.S.A.* **104**, 17650–17655 (2007).
8. T. W. B. Kibble, *J. Phys. A Math. Theor.* **9**, 1387 (1976).
9. Q. Zhou, T.-L. Ho, *Phys. Rev. Lett.* **105**, 245702 (2010).
10. A. Polkovnikov, K. Sengupta, A. Silva, M. Vengalattore, *Rev. Mod. Phys.* **83**, 863–883 (2011).
11. J. Eisert, M. Friesdorf, C. Gogolin, *Nat. Phys.* **11**, 124–130 (2015).
12. N. Navon, A. L. Gaunt, R. P. Smith, Z. Hadzibabic, *Science* **347**, 167–170 (2015).
13. L. W. Clark, L. Feng, C. Chin, *Science* **354**, 606–610 (2016).
14. J. Beugnon, N. Navon, *J. Phys. At. Mol. Opt. Phys.* **50**, 022002 (2017).
15. A. Keesling *et al.*, *Nature* **568**, 207–211 (2019).
16. M. Prüfer *et al.*, *Nature* **563**, 217–220 (2018).
17. S. Erne, R. Bücker, T. Gasenzer, J. Berges, J. Schmiedmayer, *Nature* **563**, 225–229 (2018).
18. J. A. P. Glidden *et al.*, *Nat. Phys.* **17**, 457–461 (2021).
19. L. Mathey, A. Polkovnikov, *Phys. Rev. A* **81**, 033605 (2010).
20. H.-C. Chu, G. A. Williams, *Phys. Rev. Lett.* **86**, 2585–2588 (2001).
21. A. J. Groszek, P. Comaron, N. P. Proukakis, T. P. Billam, *Phys. Rev. Res.* **3**, 013212 (2021).
22. S. Sunami *et al.*, *Phys. Rev. Lett.* **128**, 250402 (2022).
23. V. Berezinskiĭ, *Sov. J. Exp. Theor. Phys.* **34**, 610 (1972).
24. J. M. Kosterlitz, D. J. Thouless, *J. Phys. C Solid State Phys.* **6**, 1181–1203 (1973).
25. D. R. Nelson, J. M. Kosterlitz, *Phys. Rev. Lett.* **39**, 1201–1205 (1977).
26. Z. Hadzibabic, P. Krüger, M. Cheneau, B. Battelier, J. Dalibard, *Nature* **441**, 1118–1121 (2006).
27. Materials and methods are available as supplementary materials.
28. L. Mathey, K. J. Günter, J. Dalibard, A. Polkovnikov, *Phys. Rev. A* **95**, 053630 (2017).
29. For the range of parameters used in this work, the ratio T/T_0 has a one-to-one mapping to the peak phase-space density of the trapped gas and sufficiently represents the effect of the quench; see (*27*).
30. A. J. Barker *et al.*, *New J. Phys.* **22**, 103040 (2020).
31. T. L. Harte *et al.*, *Phys. Rev. A* **97**, 013616 (2018).
32. A. J. Barker *et al.*, *J. Phys. At. Mol. Opt. Phys.* **53**, 155001 (2020).
33. We analyzed the fringes within a region of interest corresponding to 80% of the Thomas-Fermi radius of the quasicondensate. As shown in fig. S3, this is where the interference fringes are clear and allow reliable measurements.
34. I. Boettcher, M. Holzmann, *Phys. Rev. A* **94**, 011602 (2016).
35. In fact, a combined fitting function can be used that has power-law behavior at short distances and exponential scaling at long distances, where the exponential length scale can be infinite.
36. P. Comaron, F. Larcher, F. Dalfovo, N. P. Proukakis, *Phys. Rev. A* **100**, 033618 (2019).
37. To motivate the scaling regimes, we considered a linear spectrum, $\omega_k = ck$. With this dispersion, dynamical phase factors of the form $\exp(i\omega_k t)$ are kept invariant if a $z = 1$ scaling is applied that leaves ckt invariant. Furthermore, for a spectrum that includes an additional length, r_0, such as $\omega_k = c\sqrt{k^2 + 1/r_0^2(t)}$, for long times, only the modes with $\omega \approx c/r_0(t)$ contribute to the dynamics. Here the scaling is replaced by keeping $ct/r_0(t)$ fixed, as it was demonstrated for the long-time dynamics in Fig. 2C. As discussed in the main text and shown in Fig. 4, the length scale $r_0(t)$ is related to the vortex fugacity increasing at long times.
38. X. G. Wen, *Quantum Field Theory of Many-Body Systems: From the Origin of Sound to an Origin of Light and Electrons* (Oxford Univ. Press, 2010).
39. J. Schole, B. Nowak, T. Gasenzer, *Phys. Rev. A* **86**, 013624 (2012).
40. S. Sunami *et al.*, Dataset for "Universal scaling of the dynamic BKT transition in quenched 2D Bose gases," version 3, Zenodo (2023); https://zenodo.org/records/8385524.

ACKNOWLEDGMENTS

We acknowledge discussions with J. Okamoto on theoretical analysis and thank J. Chalker for comments on our manuscript.

Funding: The experimental work was supported by the EPSRC grant reference EP/S013105/1. S.S. acknowledges the Murata Overseas Scholarship Foundation, the Ezoe Memorial Recruit Foundation, the Daishin Foundation, and St. Hilda's College, Oxford, for financial support. D.G., A.B., A.J.B., and K.L. thank the EPSRC for doctoral studentships. L.M. acknowledges funding by the Deutsche Forschungsgemeinschaft (DFG) in the framework of SFB 925 – project ID 170620586 and the excellence cluster "Advanced Imaging of Matter" – EXC 2056 – project ID 390715994. V.P.S. acknowledges funding by the Cluster of Excellence "QuantumFrontiers" – EXC 2123 – project ID 390837967. **Author contributions:** S.S. performed the experiments and data analysis. V.P.S. and L.M. developed numerical and analytical models and contributed to the interpretation of our experimental data. S.S. and V.P.S. wrote the manuscript. L.M. and C.J.F. supervised the project. All authors contributed to the discussion and interpretation of our results. **Competing interests:** The authors declare that they have no competing interests. **Data and materials availability:** All data presented in this paper and numerical simulation codes are available at Zenodo (*40*).

SUPPLEMENTARY MATERIALS

science.org/doi/10.1126/science.abq6753
Materials and Methods
Figs. S1 to S9
References (*41*–*54*)

Submitted 11 May 2022; accepted 16 September 2023
10.1126/science.abq6753